RSC Applied Polymers

PAPER

View Article Online
View Journal | View Issue

Cite this: *RSC Appl. Polym.*, 2026, **4**, 807

Effect of corona charging, additives and processing conditions on the barrier and filtration properties of polypropylene melt-blowns

Partha Sikdar * and Gajanan S. Bhat

Air pollution and airborne pathogens pose significant risks to public health and well-being. Electret melt-blown filters with high filtration efficiency (FE) and low-pressure drop (PD) are used to prevent inhalation of these pollutants. Melt-blown polypropylene (PP) electret filters offer an attractive combination of fine-fiber structure and electrostatic particle capture but often provide limited charge stability and inconsistent performance. In this study, we investigated the combined effects of corona charging, magnesium stearate (MgSt) additive loading, and melt-blown processing conditions on the filtration behavior and long-term stability of PP melt-blown. Melt-blown webs were produced using controlled variations in air pressure, die-to-collector distance (DCD), and MgSt concentration (0–2 wt%), followed by corona treatment at −50 kV. The incorporation of MgSt significantly increased the surface charge density, leading to substantial improvements in post-charging filtration efficiency (FE). All charged samples achieved FE values exceeding 98% at 32 L min^{-1}, with quality factor (QF) values improving by 2–5 times compared to uncharged webs. Samples containing 1 wt% MgSt exhibited the optimal balance of FE, pressure drop (PD), and electret stability, demonstrating minimal performance decay over 60 days. Structural analysis using scanning electron microscopy (SEM), porometry, differential scanning calorimeter (DSC), and X-ray diffraction (XRD) revealed that MgSt acted as a heterogeneous nucleating agent, increasing crystalline interfaces and enabling deeper charge-trap formation. These findings indicate that the combination of MgSt with optimized processing and corona charging offers a practical route to produce high-efficiency, low-resistance melt-blown electret filters with improved long-term performance.

Received 19th July 2025,
Accepted 15th January 2026

DOI: 10.1039/d5lp00221d

rsc.li/rscapplpolym

Introduction

Air pollution and airborne diseases have drawn worldwide attention in recent years due to their severe threat to public health, climate and ecosystems.[1–3] Airborne diseases like the coronavirus have caused major disruptions to nearly all facets of daily life around the world, affecting everything from healthcare systems to economic stability and social interactions.[4] Airborne diseases are primarily transmitted through aerosol droplets released when an infected person coughs, sneezes, talks, or breathes. Research has shown that these droplets can remain suspended in the air for extended periods, increasing the risk of transmission in enclosed spaces. However, despite ongoing research and trials, an effective method for completely mitigating airborne diseases has not yet been developed. Current preventive approaches include wearing personal protective masks, such as N95 respirators, which are designed to filter out at least 95% of airborne particles, providing a higher level of protection compared to standard cloth masks. Fine particulate matter (PM ≤ 2.5 μm) consists of tiny particles that can penetrate deep into the lungs and even enter the bloodstream, leading to various health issues, including respiratory and cardiovascular diseases. Furthermore, air pollution has raised concerns about exacerbating health risks. Research indicates that areas with high levels of air pollution may experience more severe outcomes for respiratory patients, as underlying respiratory conditions can worsen the effects of the virus.[5,6]

To contextualize performance standards, the efficiencies of respirators, surgical masks, and cloth masks have been compared in previous work. N95 and KN95 respirators exhibited PDs ranging from 125 to 200 Pa, which remained well below the NIOSH limit of 343 Pa, and achieved filtration efficiencies of 83–99% for particles with a diameter of 300 nm. In contrast, surgical masks showed much lower PDs (35–55 Pa) but moderate FE, averaging 88% for the best-performing mask and 42–62% for other surgical samples. The superior performance of surgical masks was related to the inclusion of a fine "submicron dust filtration layer", which enhanced capture efficiency without greatly increasing resistance. Surgical masks often

Department of Textiles, Merchandising and Interiors, University of Georgia, Athens, GA, USA. E-mail: ppprs92@gmail.com

consist of fine submicron dust filtration layers that provide higher filtration performance. Cloth masks and bandanas provide the lowest efficiencies (<25%) with low PDs (10–50 Pa), showing a clear trade-off between breathability and particle capture. Doubling or layering masks improved FE but also increased PD. Overall, N95 respirators have the highest QF (QF $\approx$ 25 kPa^{-1}), followed by surgical masks ($\approx$23 kPa^{-1}), KN95 respirators ($\approx$15 kPa^{-1}), cloth masks ($\approx$12 kPa^{-1}), and bandanas ($\approx$3 kPa^{-1}). Despite exhibiting lower efficiency than N95s, surgical masks displayed higher QF values due to their much lower PD, highlighting the importance of balancing filtration and airflow resistance in evaluating the overall mask performance.[7]Electret filters are popular in PM filtration and virus defense due to their low cost, energy efficiency, high FE, and low PD, making breathing easier.[5] The electret melt-blown nonwoven filter is primarily used in respirators for its fine diameter, small pore size, high porosity, 3D structures, and quasi-permanent electrostatic interaction.[8] This material has a unique electrostatic filtering mechanism to capture viruses (approximately 100 nm) through electrostatic attraction. The FE of the electret melt-blown nonwoven filter is significantly enhanced without increasing the PD, making it ideal for surgical masks, air-purifying respirators, HVAC filters, and automotive cabin air filters.[9]The performance of electret melt-blown filters relies on the amount and duration of the implanted charges, which determines the strength of the electrostatic attraction. Currently, there are two main approaches to enhance electret performance. The first approach involves blending additives with a polymer during the melt-blown process. This optimization of the material's crystal structure creates more sites for charge storage. The second approach focuses on improving charging technology by optimizing charging parameters. Electret filters can be produced using various methods, including corona, triboelectric, induction, and water jet charging. The corona charging is the most commonly used among these methods, as it is suitable for charging all types of fibers.[10] Corona discharge occurs when a high electric field is applied between two asymmetric electrodes.[11] The key factors influencing this process include applied voltage, charging time, distance, and environmental conditions.[12] When increasing the applied voltage and charging time, the surface voltage of electret materials is boosted, while charging distance negatively affects it.[11] Thakur *et al.* noted a threshold for applied voltage that varies by charging polarity.[11] Additionally, optimal thermal treatment and storage conditions can enhance charge stability in electret materials. While these studies focused on the relationship between FE and process factors, the stability of FE itself remains underexplored.[13]The charge of electret materials will decay after a certain period of time, and the charge storage stability hinders the filtration performance of the electret filters significantly.[14] To reduce the charge decay, several researchers attempted to charge the material under variously elevated thermal conditions. The surface voltage of a PP nonwoven filter increased with the charging temperature, and the highest surface voltage was obtained at 50 °C and 130 °C.[15,16] Due to bulk conductivity, surface conductivity, and ionic attacks from the surrounding environment, charge decay is inevitable over time, leading to a significant reduction in FE.[17] Several efforts have been made to enhance filtration performance by incorporating additives into the polymer. Yu *et al.* introduced tourmaline particles into polylactic acid (PLA) to create melt-blown nonwovens, achieving an FE of 88%. The improvement of increased friction between the fiber web and the tourmaline particles enhanced the electrostatic adsorption capacity of the melt-blown nonwoven particles.[18] Similarly, PP electret melt-blown nonwovens containing barium titanate particles, achieved an impressive FE of 99.97% at a PD of 95 Pa. This exceptional performance is due to the dielectric properties of barium titanate, which increases localized polarizability within the polymer due to its high dielectric constant.[14] Brochocka *et al.* developed electret perlite-modified PP melt-blown nonwovens that demonstrated an FE of 99.56% with a PD of 290 Pa.[19] The FE of electret melt-blown nonwovens can be significantly improved by incorporating additives into the polymers. However, these materials still face several challenges, including relatively high filtration resistance, fast charge decay and higher PD. Some studies have tackled this problem by optimizing the structure of the materials. Furthermore, the stability of the electret, especially its low filtration stability under high temperature and humidity conditions, limits its applications. Therefore, there is a pressing need to develop electret materials for air filtration that offer low air resistance and excellent charge retention.[20,21] Xiao *et al.* approached tackling these problems by incorporating MgSt into PP melt-blowns. The produced melt-blown achieved filtration efficiencies of 99.68% and 99.43%, respectively.[22] The studies of their multi-layered designs improved particle capture and reduced airflow resistance through architectural layering and optimized charging parameters; however, they did not address the persistent challenge of charge decay over time.[22] Although several studies have explored the optimization of melt-blown structures and charging conditions to increase FE, limited attention has been given to the long-term electrostatic stability and the interplay between material formulation and processing parameters. Previous works on multi-layered or corona-charged melt-blown filters primarily emphasized structural design and short-term performance, often overlooking charge-decay behavior and additive-assisted charge stabilization. However, there is still a need for comprehensive studies that systematically examine the combined influence of melt-blown processing parameters including air pressure and DCD, corona charging distance, and the incorporation of magnesium stearate (MgSt) into PP on FE, PD performance, and charge retention over extended periods.

This study presents a clear approach to developing high-performance melt-blown filtration materials by optimizing processing conditions and integrating corona charging technology. The resulting materials demonstrate excellent electret properties for up to 60 days with more than 99% FE, and air permeability of 43 $m^3\ s^{-1}\ cm^{-2}$. MgSt particles were introduced as charge enhancers during the melt-blown process to enhance crystal structure and improve electret behavior. By

optimizing the MgSt ratio, PP/MgSt electret melt-blown nonwoven filters were successfully fabricated. The structural characteristics, filtration performance, and underlying mechanisms for performance enhancement were systematically investigated. Furthermore, a comprehensive analysis of corona charging conditions and long-term charge decay behavior was conducted to establish the correlation between processing parameters, electret stability, and filtration performance.

Materials and methods

Preparation of melt-blown webs

PP granules (Metallocene PP, MF650X, LyondellBasell) were used as the base polymer for melt-blown fabrication. The resin exhibits a narrow molecular weight distribution, a melt flow rate of 1200 g per 10 min (ASTM D1238), and a melting range of 145–165 °C. The physical properties of the PP are presented in Table 1.

All melt-blown webs were produced using a 600 mm pilot melt-blowing line at the Nonwovens Research Laboratory as depicted in Fig. 1a (University of Georgia). The air heater temperature was maintained up to 315 °C, and an oil-free compressor supplied air pressures up to 1.5 bar. The die was an Exxon-style linear die with 20 holes per cm and a nominal throughput of 0.4 g per hole per min.

Incorporation of additives in melt-blown nonwoven webs

A masterbatch containing MgSt from Standridge was incorporated into the PP polymer to investigate its effects on barrier properties, filtration, and electret characteristics. The masterbatch was dry blended with PP homopolymer (density 0.93 g cm^{-3}), and its physical properties are summarized in Table 2.

To prepare the final formulations, the 10 wt% MgSt masterbatch was mixed with neat PP to obtain MgSt concentrations of 1 wt% and 2 wt%. This corresponded to blend ratios of 10 : 90 (masterbatch : PP) for 1 wt% MgSt and 20 : 80 for 2 wt% MgSt. Mixing was performed using a BILT HARD portable mixer under controlled shear conditions, with residence times of 30–90 seconds and specific mixing energies of 0.3–1.0 kWh kg^{-1}. These conditions ensured effective breakup of agglomerates, uniform dispersion of MgSt within the polymer matrix, and preserved thermal stability of the resin. Based on initial processing trials, an air pressure of 50 kPa and a die-to-collector distance (DCD) of 15 cm produced the highest filtration efficiency (FE) with minimal pressure drop (PD). Hence, these parameters were selected as the baseline for evaluating MgSt effects.

Table 1 The typical properties of the PP used in melt-blowing

Properties	Value
Melt flow rate (230 °C per 2.16 kg) (ASTM D1238)	1200 g per 10 min
Density (23 °C) (ASTM D792)	0.90 g cm^{-3}
Melting point	145 °C–165 °C
Appearance	White granules

Using the optimized conditions, LyondellBasell PP was melt-blended with the MgSt masterbatch to produce six melt-blown samples (Table 3), containing either 1 wt% or 2 wt% MgSt. Most samples were processed at 50 kPa; however, samples E45.15-1 and E48.15-1 were produced at slightly different air pressures of 45 kPa and 48 kPa, respectively, to examine pressure-related effects. During melt-blowing, the die, melt, and air temperatures were maintained between 230 and 240 °C, and the extruder operated at 31–35 rpm.

Corona charging of melt-blown nonwovens

All melt-blown samples were corona-charged as shown in Fig. 1b, using a −50 kV DC voltage applied through a point-to-plane electrode configuration at a conveyor speed of 2 m min^{-1}. Charging distances of 3, 5, and 7 cm were evaluated, with environmental conditions held at 25 ± 2 °C and 40 ± 5% RH. After charging, samples were handled with nitrile gloves and stored on a wooden rack for up to 60 days to evaluate charge decay. Surface charge was measured every 15 days.

Characterization of electret nonwovens

The weights of the melt-blown nonwoven webs expressed as gram per square meter were determined according to the method of ISO 3801. Air permeability was determined using a TEXTEST FX3330 air permeability tester, according to ASTM D73796. The hydrostatic head was measured according to AATCC 127 using a TEXTEST FX 3000 tester. The mean flow pore diameter, smallest pore diameter, bubble point pore diameter, and pore size distribution of the samples were characterized using a Capillary Flow Porometer in accordance with ASTM F316-03 (2011). The bubble point refers to the largest pore through which the first detectable air bubble passes when the sample is wet. The mean pore diameter is determined from the peak of the flow distribution curve, while the smallest pore diameter is defined as the pore that closes under the maximum applied pressure. The surface morphology of melt-blown nonwovens was investigated using a scanning electron microscope under 5–10 kV voltage and operated at various magnifications. The fiber diameters and their size distribution were calculated using ImageJ software and Origin Pro 2023 by measuring 200 fibers from the various SEM images. An automated FE tester (TSI 8130, TSI Instruments Co. Ltd) was used for evaluating the filtration performance of melt-blown nonwovens. In the current study, sodium chloride was used to generate aerosol particles with a mass median diameter of 0.26 nm using an atomizing air pump. The particles' geometric standard deviation was less than 1.86%. At an air flow rate of 32 L min^{-1}, the sample size was 100 cm^2. For each sample, measurements were made in ten different places.

The FE is calculated as follows:

$$\eta = 1 - \varepsilon_1/\varepsilon_2$$

where η represents the FE, and ε_1 and ε_2 are the quantity of the aerosol particles downstream and upstream of the filter, respectively. The PD of the sample was measured by a flow gauge and two electronic pressure transmitters. The test process was con-

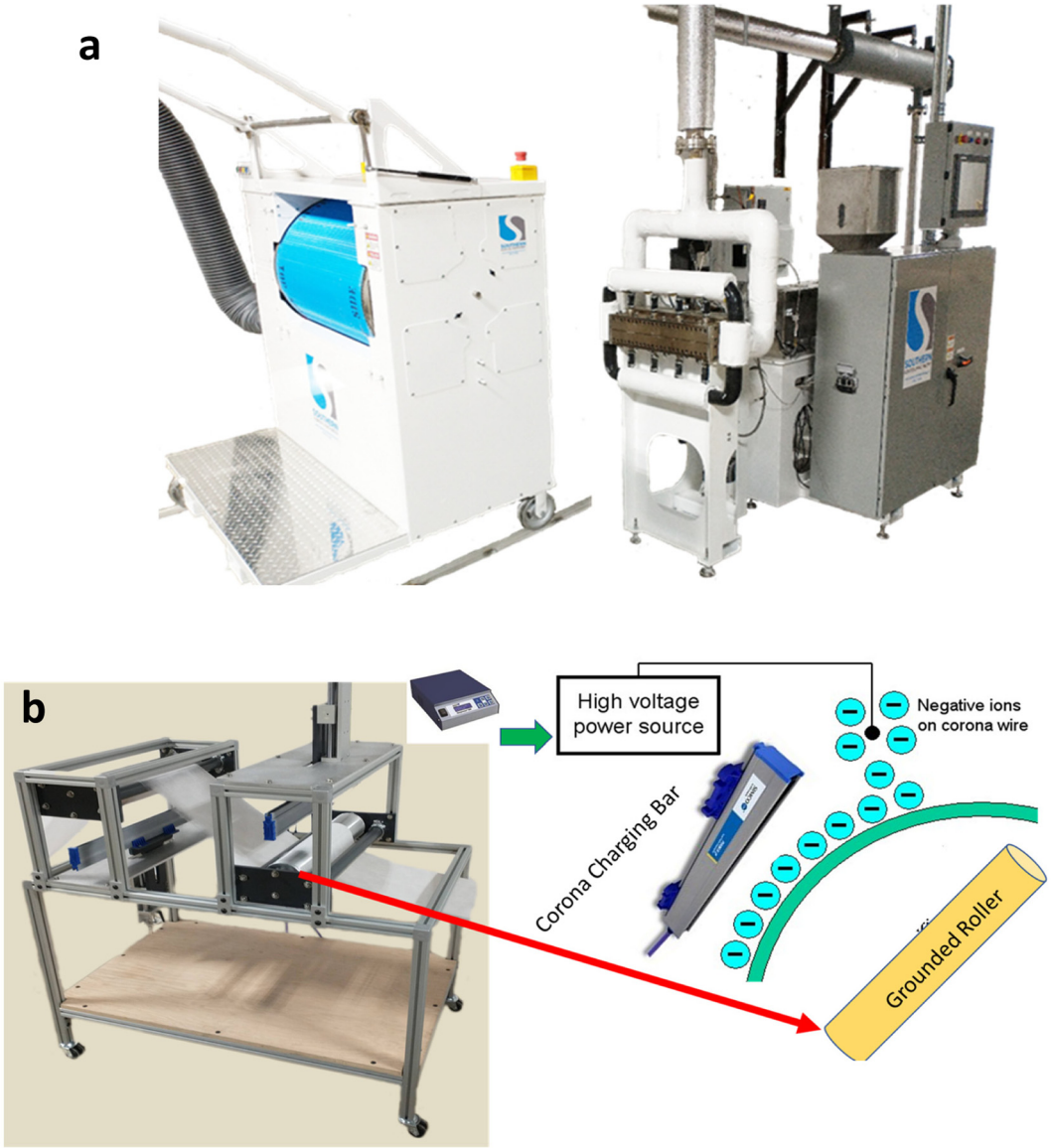

Fig. 1 (a) Melt-blowing pilot line and (b) the corona charging procedure.

Table 2 Physical properties of the masterbatch

Properties	Value
Melt flow rate (230 °C per 2.16 kg) (ASTM D1238)	50 g per 10 min
Density (23 °C) (ASTM D792)	0.95 g cm^{-3}
Heat stability	260 °C
Appearance	Semi-transparent pellets

ducted at an ambient temperature of 25 ± 2 °C and a relative humidity of 45 ± 5%. The quality of a filter media can be assessed by the QF. The QF is defined as:[23]

$$QF = \frac{-\ln P}{\Delta p} \quad (1)$$

where P is the penetration fraction, and Δp is the PD across the medium.

The surface charge and voltage were measured using a non-contact Nanocoulomb Meter (Model 230, ETS, USA) and an Electrostatic Field Meter. The ETS Model 230 Nanocoulomb Meter was calibrated using the built-in CAL output and test capacitor, and the readings were confirmed within the acceptable accuracy range (5%). Charge measurements were taken using the probe in direct-contact mode, ensuring consistent probe placement for repeatability. The FMX-004 Electrostatic Field Meter was also calibrated by allowing a 10-minute stabilization period, then applying known electrostatic field levels at the standard 1-inch standoff. Readings at multiple setpoints (±0.5, ±1, ±2, and ±5 kV) were compared with the reference values to confirm accuracy. The tests were conducted at an

Table 3 The details of the process parameters to produce melt-blown nonwovens with Mg-stearate

Sample	Grams per square meter/ GSM ($g\ m^{-2}$)	Air pressure (kPa)	DCD (cm)	Percentage of MgSt (%)	Thickness (mm)
P50.15	33	50	15	0	0.35
S50.15-1	34.3	50	15	1	0.34
S50.15-2	34.7	50	15	2	0.30
E45.15-1	35	45	15	1	0.31
E.48.15-1	35	48	15	1	0.34
P50.20	35	50	20	0	0.41
S50.20-1	34.7	50	20	1	0.36
S50.20-2	34.7	50	20	2	0.30

ambient temperature of 25 ± 2 °C and relative humidity of 45 ± 5%. For each sample, ten measurements were taken in different spots on the web. The charge durability was measured by storing the charged melt-blown nonwovens for 60 days and testing them at fixed time intervals.

A differential scanning calorimeter (Mettler Toledo DSC 821e) was used to study the thermal properties of specimens and the changes in crystallinity. A heating rate of 10 °C min^{-1} was used between 30 °C to 230 °C in the presence of inert gas (N_2) at a flow rate of 100 cc min^{-1}. The degree of crystallinity (X_c) was calculated using eqn (2):[24,25]

$$X_c = \frac{\Delta H_c}{\Delta H_{100}} \times 100 \quad (2)$$

where ΔH_c is the melting enthalpy of the produced melt-blown PP specimen and ΔH_{100} (207 J g^{-1}) is the melting enthalpy of 100% crystalline PP.

The Bruker D8 Advance instrument (Bruker, USA), which operates with a CoKα1 radiation source (λ = 1.79 Å) at 35 kV and 40 mA, was used to detect the crystalline phase composition and crystallinity. X-ray diffraction (XRD) patterns were recorded by scanning at 2θ = 5° to 35°, with a step size of 0.01° and a scanning rate of 0.1 s per step. A silicon wafer was placed in the specimen holder of the XRD machine to perform the measurements. The samples were cut into pieces ~20 mm long and mounted side by side on the silicon wafer (~15 mm wide). The Scherrer equation was used to calculate crystallite size:

$$D = \frac{K\lambda}{\beta \cos I} \quad (3)$$

where D = crystallite size (nm), K = 0.9 (Scherrer constant), λ = wavelength of the X-ray source, θ = peak position, and β = full width at half maximum of peaks (in radians) located at any 2θ in the pattern.

Statistical analysis

A paired t-test was performed to evaluate the effect of corona charging on the quality factor (QF). The test compared the QF of each sample before and after charging, treating measurements from the same sample as paired observations. Statistical significance was set at $p < 0.05$. All analyses were conducted using Origin Pro.

Results and discussion

Effect of corona charging on barrier and filtration properties of polypropylene melt-blowns

Surface charge and voltage. To investigate the influence of charge distribution on the efficiency of filtration, a series of tests were conducted to evaluate the surface potential and surface charge of the melt-blown nonwovens. Fig. 2a illustrates the findings, which reveal a diverse range of surface potentials ranging from −21.5 kV to −9.8 kV. Furthermore, an analysis revealed that the surface charge varied between −98 nC and −155 nC. Sample P65.15 had the higher surface charge of −155 nC and surface voltage of −21.5 kV, respectively, whereas P35.15 showed the lowest value of both surface charge and voltage.

Filtration efficiency and pressure drop. The uncharged melt-blown webs have moderate filtration efficiencies (45–65%) due to their reliance solely on mechanical interception (Fig. 2b). As expected, particles smaller than 0.3 μm are particularly challenging to capture because their size approaches or falls below the characteristic fiber diameters of melt-blown media. To overcome this limitation, corona charging is widely employed to introduce quasi-permanent electrostatic charges that significantly enhance particle capture without increasing fiber packing density or airflow resistance. Applying a −50 kV corona charge at an electrode distance of 7 cm and a web speed of 2 m min^{-1} nearly doubled the FE of all samples. After charging, every melt-blown web achieved FE values exceeding 98% at a flow rate of 32 L min^{-1}. Sample P65.15 showed the best performance with an FE of 99.1% and a PD of 49 Pa, which correlates with its higher measured surface charge. Conversely, P35.20 displayed a slightly lower FE of 97.8% but maintained a lower PD of 31 Pa, demonstrating the tunability of filtration properties through process conditions. Importantly, corona charging had a minimal effect on PD. As shown in Fig. 2c, PD values remained within a comfortable breathing range (17–49 Pa), indicating that the applied voltage did not change pore size or fiber morphology. Consequently, the QF improved markedly, increasing by 2–5 times relative to uncharged samples (Fig. 2d). These results confirm that corona charging is a highly effective strategy for significantly enhancing FE while preserving low airflow resistance and respiratory comfort.

Mechanism of improving filtration efficiency. Negative corona discharge happens when a sharp electrode (*e.g.*, a needle or wire) relates to a high negative potential relative to a grounded or less negative counter-electrode, as illustrated in Fig. 3a. The intense electric field at the electrode tip causes field emissions of electrons, which collide with air molecules, and induces an electron flow and ionization process. The collision generates charge carriers with electrons and negative ions (such as O^-, O_2^-). These carriers drift away from the elec-

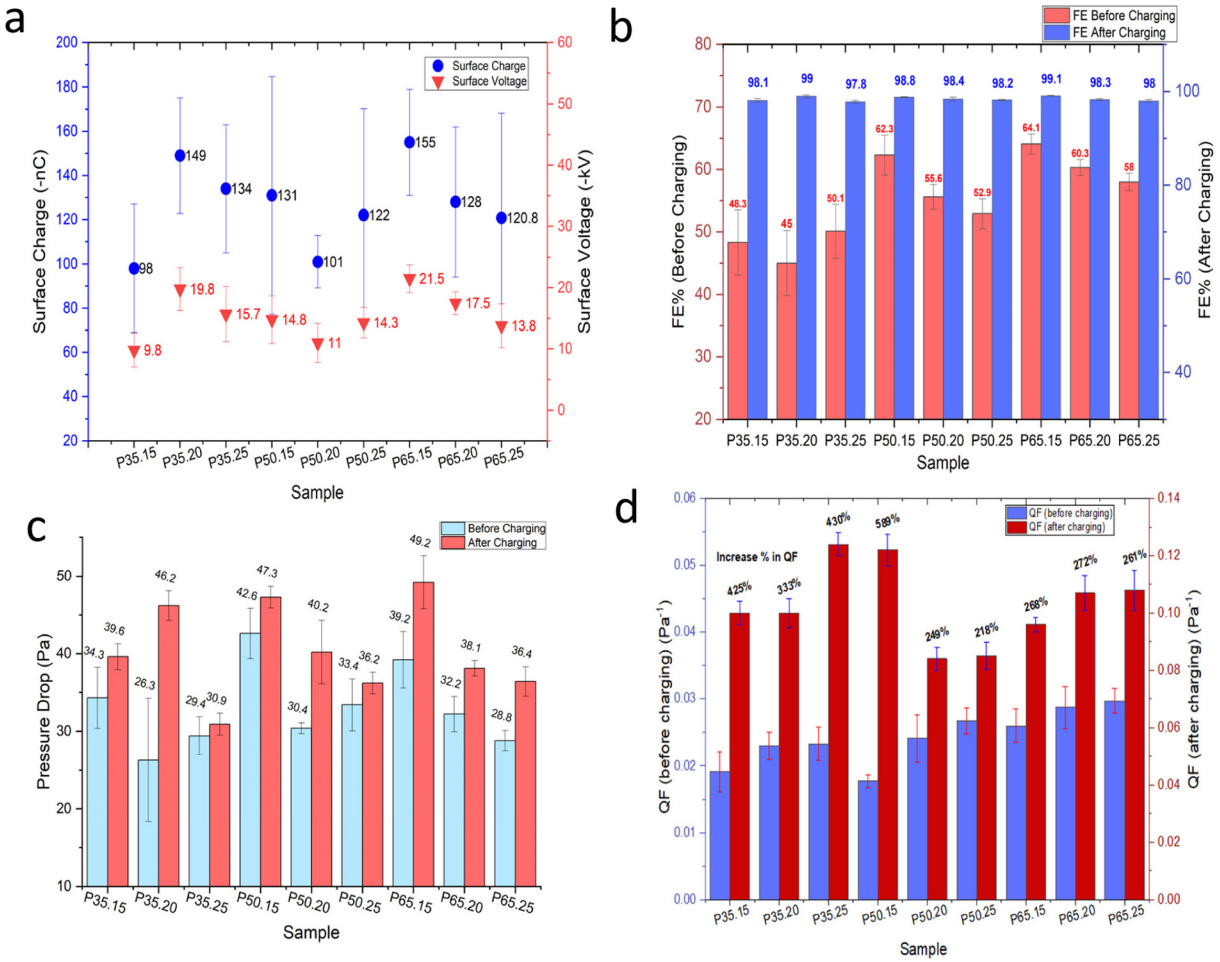

Fig. 2 (a) The surface charge and voltage of MB samples. (b) Filtration efficiency after corona charging at −50 kV voltage and 7 cm distance. (c) Pressure drop after corona charging at −50kV voltage and 7 cm distance. (d) Quality factors of different melt-blown samples.

trode toward the grounded surface under the influence of the electric field. During this process, the negative ions and electrons can deposit onto nearby dielectric surfaces (*e.g.*, polymer fibers in a melt-blown nonwoven) and become either surface charges or trapped charges when entering defect sites, voids, or interfacial regions within the material. The accumulation of these charges imparts an internal or surface electric field to the polymer, turning it into an electret. Charging stability in a negative corona-charged electret depends strongly on trap depth, polymer microstructure, humidity, and temperature. The electrons and negative ions tend to occupy shallower traps and have higher mobility.[26,27] Polymeric electret fabrics are charged through induced or oriented dipoles within the polymeric material and ideally retain their static charge.[28]

Effect of charging distance on the filtration efficiency and surface charge

The effect of corona charging distance on electret performance was examined by adjusting the gap between the corona electrode and the grounded roller to 3, 5, and 7 cm. During charging, the uncharged nonwoven material was passed at a speed of 2 m min^{-1} under a constant negative voltage of −50 kV. Four melt-blown samples (P50.20, S50.20-1, E45.15-1, and E48.15-1) were evaluated. As presented in Fig. 3b, the highest filtration efficiencies of 99.4%, 99.2%, 98.4%, and 96.7%, respectively, were achieved at a charging distance of 7 cm. A similar trend was observed for surface charge density (Fig. 4). At 7 cm, sample P50.20 exhibited the highest surface charge of −145 nC, followed by S50.20-1 at −102 nC. When the charging distance was reduced to 3 cm, the surface charge significantly decreased, with P50.20 and S50.20-1 showing only −18 nC and −79 nC, respectively.

These results suggest that electrode distance plays a crucial role in the effective charge deposition and electret formation. At a very short distance (*e.g.*, 3 cm), the electric field becomes excessively intense, leading to harsh ion bombardment that can cause local fiber melting, micro-arcing, and uneven surface charging. Under such conditions, charges tend to accumulate only on the fiber surface, occupying shallow traps and resulting in weaker and less durable electret behavior. In contrast, a 7 cm gap provides an optimal balance between elec-

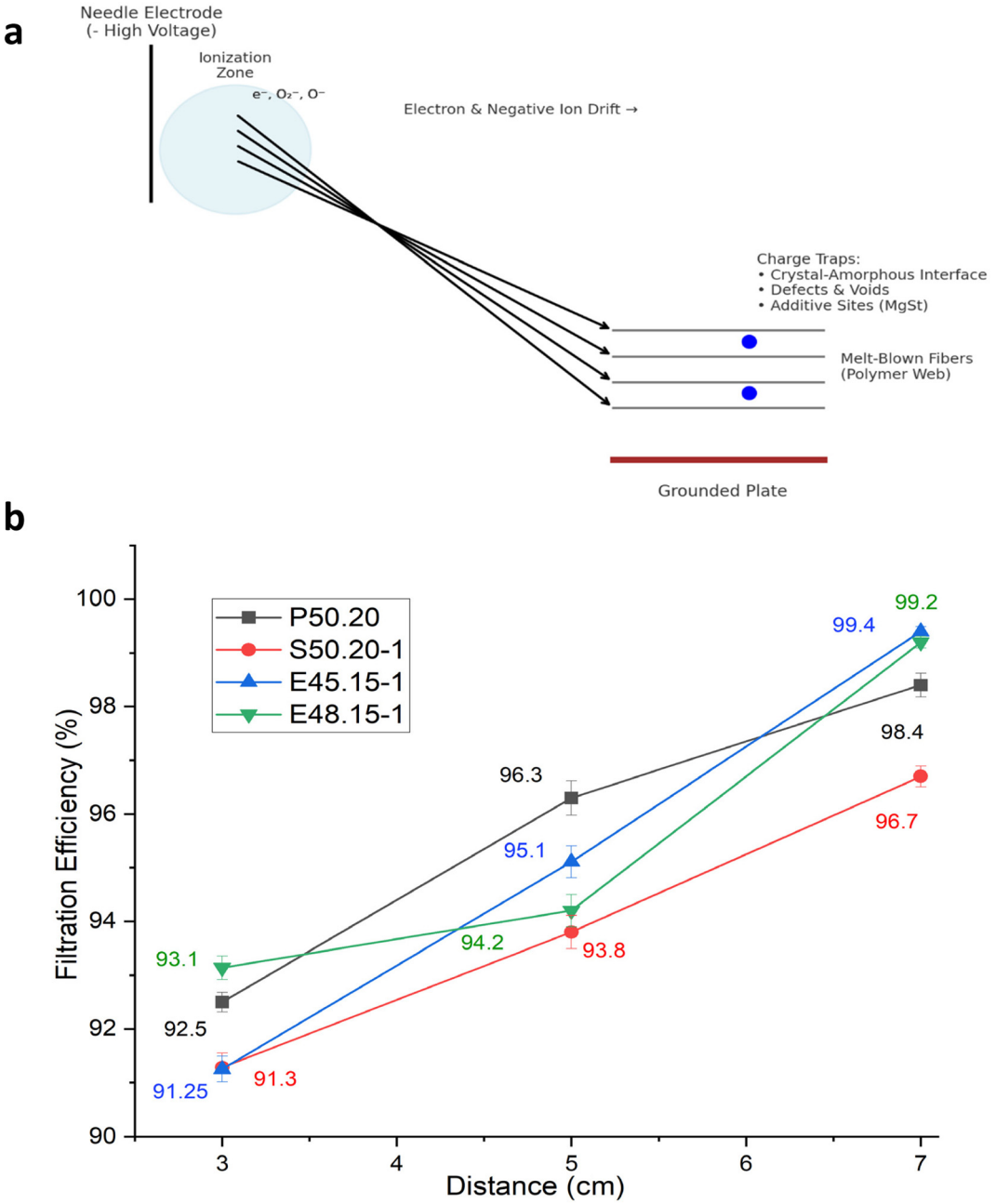

Fig. 3 (a) Corona charging mechanism and (b) effect of corona charging distance on filtration efficiency of MB nonwovens.

tric field strength and ion mobility, enabling ions to disperse and deposit uniformly into deeper trap sites within the fiber structure, thereby enhancing charge retention. When the distance exceeds the optimal range, the electric field weakens, and ion recombination becomes more likely before reaching the fiber surface, ultimately reducing charge deposition and electret performance. These observations are consistent with previous studies, which report an optimal corona charging distance of approximately 7–8 cm for melt-blown electret filtration materials.[29,30]

Effect of additives on barrier, electret properties of polypropylene melt-blowns

Fiber morphology and diameter distribution. The microstructure of the samples can be observed in the SEM micrographs (Fig. 5). The representative SEM images reveal that the fibers in all samples were uniformly dispersed in a random manner. In the case of samples P50.15 and P50.20, the fibers display less variation in size, resulting in relatively compact and dense fabrics (Fig. 6). Conversely, in samples S50.15-2,

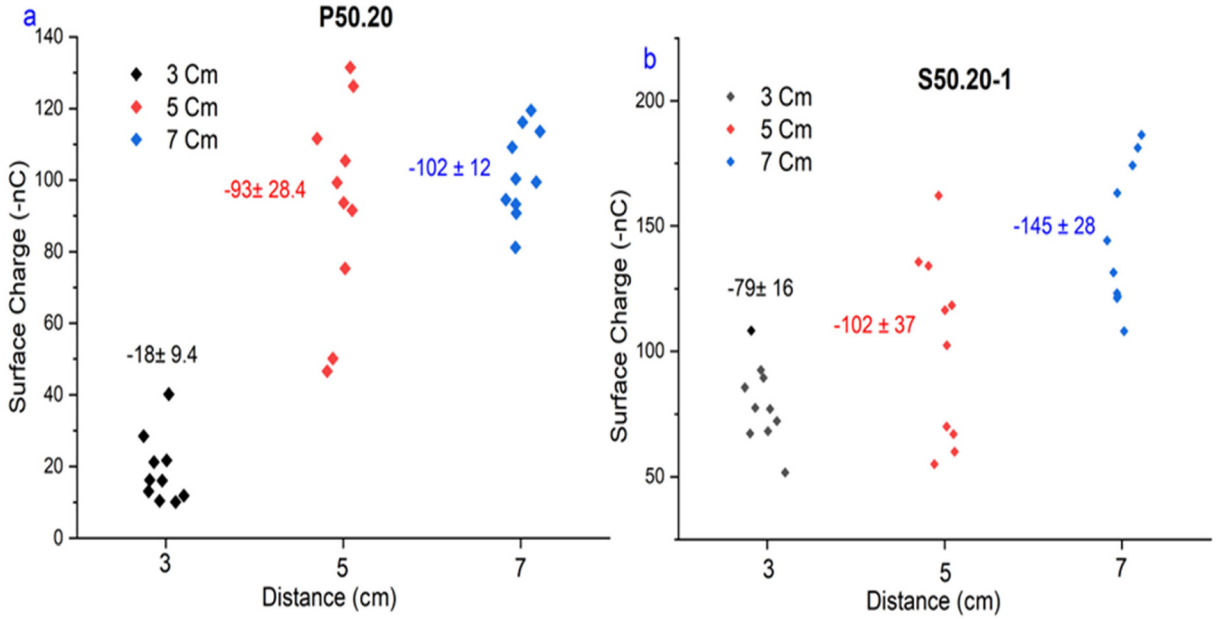

Fig. 4 Mean surface charge measured in nanocoulomb meter: (a) P50.20; (b) S50.20-1.

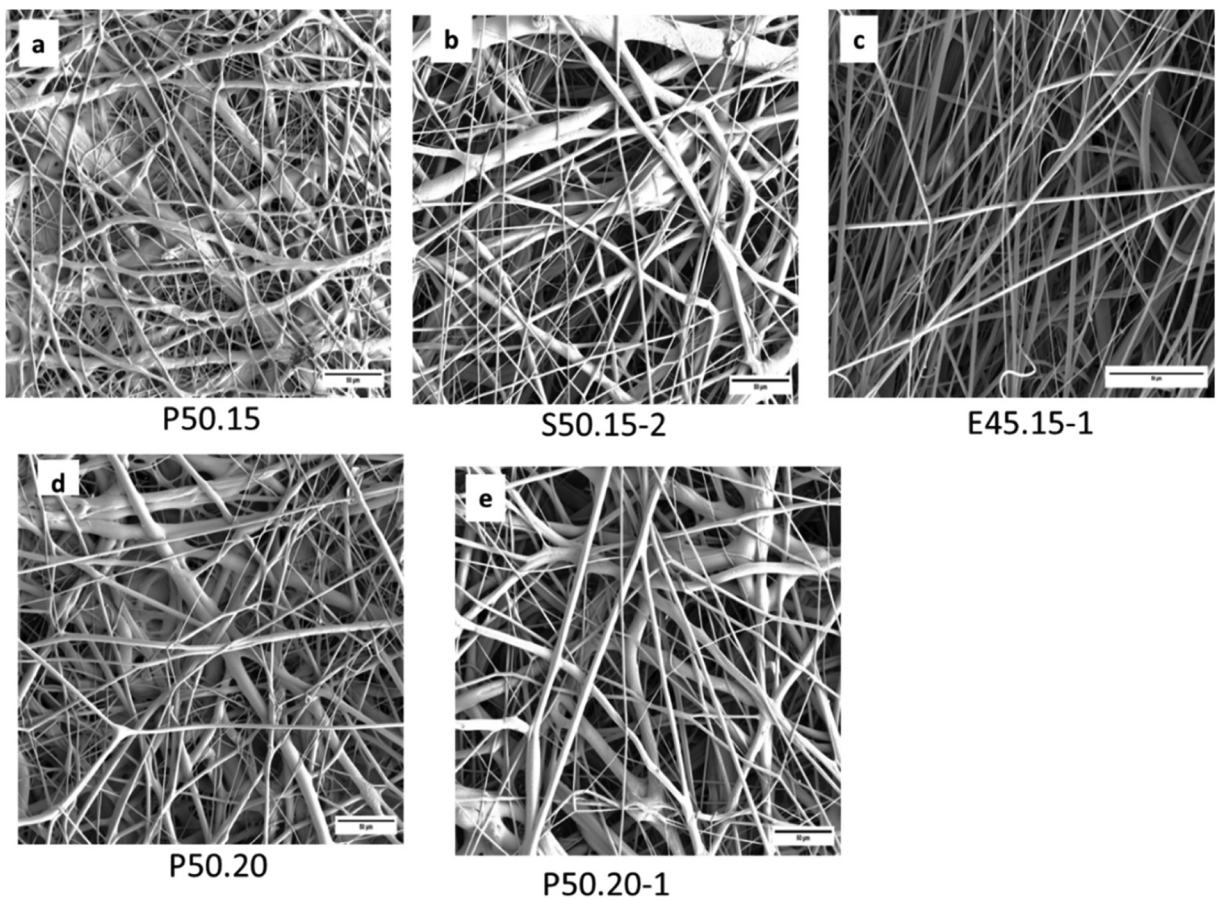

Fig. 5 SEM micrographs of fibers with and without additives (a–e).

S50.20-2 and E45.15-1, the fibers exhibit a relatively more uniform size, leading to fabrics that appear relatively loose in structure with more open structure among fibrous networks.

Additionally, the PP/MgSt samples exhibited smooth surfaces without any noticeable agglomerates. This favorable outcome can be attributed to the efficient melting and mixing of the masterbatch with MgSt at higher process temperatures, facilitating their uniform dispersion within the molten PP. MgSt particles were introduced into the extruder in conjunction with the PP chips throughout the melt-blown process. The melting point of MgSt is approximately 200 °C, and the extruder operates at temperatures exceeding 232 °C, allowing this high temperature environment effectively to allow for complete melting and integration of these beneficial MgSt particles during this intricate procedure. In contrast to inorganic particles like barium titanate,[14,31] tourmaline,[32] and TiO_2 particles[33] that tend to aggregate on the fiber surface, the MgSt particles were successfully melt-mixed with the PP without forming any agglomerates. Additionally, the average fiber diameters of the samples produced with additives ranged from

Table 4 Pore and fiber diameter of melt-blown nonwovens

		Pore diameter (μm)		
Sample	Fiber diameter (μm)	Mean	Bubble point	Smallest
P50.15	3.42 ± 1.2	8.8	15.5	4.3
S50.15-1	3.64 ± 1.27	14.3	22.5	6.6
S50.15-2	3.7 ± 2	16.0	23.9	9.5
E45.15-1	1.8 ± 0.25	11.9	20.0	6.8
E.48.15-1	2.3 ± 0.91	12.7	20.6	6.7
P50.20	2.7 ± 1.2	10.2	17.3	6.5
S50.20-1	3.1 ± 1.35	17.2	26.5	6.5
S50.20-2	3.5 ± 1.60	19.8	29.0	18.9

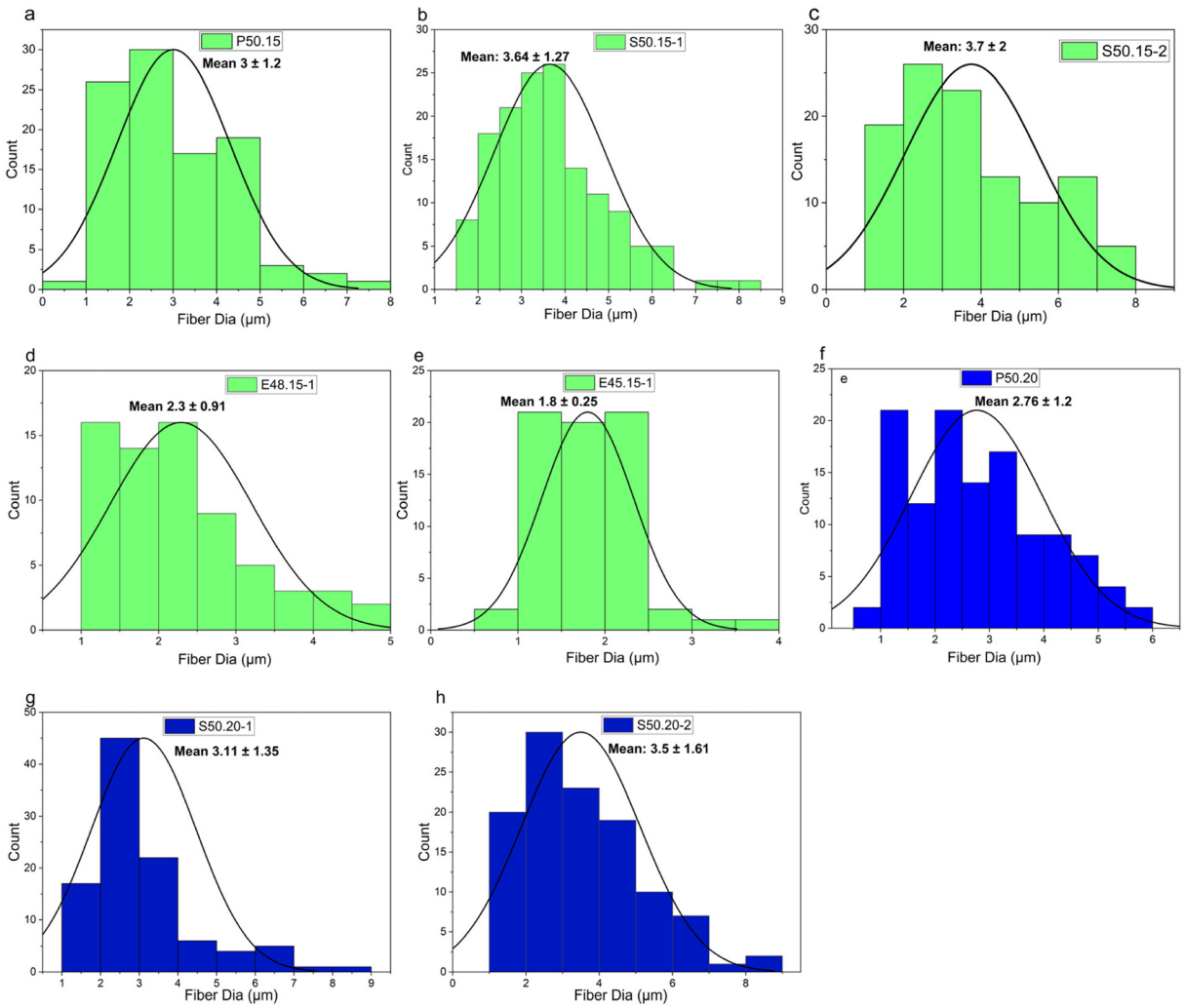

Fig. 6 SEM micrographs of fibers with and without MgSt additive: (a) sample produced at 50 kPa air pressure and 15 cm DCD without additive; (b) sample produced at 50 kPa air pressure and 15 cm DCD with 2 wt% MgSt; (c) sample produced at 45 kPa air pressure and 15 cm DCD with 1 wt% MgSt; (d) sample produced at 50 kPa air pressure and 20 cm DCD without additive; (e) sample produced at 50 kPa air pressure and 20 cm DCD with 1 wt% MgSt.

3.7 to 1.8 μm, as indicated in Table 4. On average, the presence of additives leads to a slight increase in fiber diameter.

Porosity and mean pore diameter. Further investigation was carried out to analyze the pore size, pore size distribution, and porosity of the samples. In the absence of additives, the mean pore diameter of the sample measured 8.8 μm and 10.2 μm. However, when additives are introduced, the average pore diameter increases between 11.9 and 19.8 μm as shown in Fig. 7a. These results imply that these additives contribute to an increase in pore size on average, which is also consistent with an increase in fiber diameter. However, the increase in pore size is much larger than the corresponding increase in fiber diameters, indicating that the result is due to a combination of several factors affecting fiber diameter and web consolidation.

P50.15 and P50.20 have pore sizes ranging from 4–15 μm and 6–16 μm, respectively. Although the densities of the samples produced are nearly identical, those produced with additives exhibit larger pore sizes, ranging from 6 to 28 μm (Fig. 7a). Moreover, the average pore diameter of the produced melt-blown nonwovens aligns closely with that of commercial samples, which typically range from 10.4 to 15 μm in size. The produced MB webs possess comparable porosity and filtration capabilities to that of commercially available fabrics. Furthermore, Fig. 7b illustrates that the porosities of the sample range from 87.7% to 90.8%. The findings indicate that all six nonwovens exhibited substantial porosity, with no significant differences observed. This corresponds to the inherent nature of melt-blown nonwovens, which are recognized for their considerable porosity.

Air permeability. To understand how the observed changes in pore structure affected airflow resistance, air permeability was measured. Air permeability varied notably among the produced melt-blown webs and was strongly influenced by the

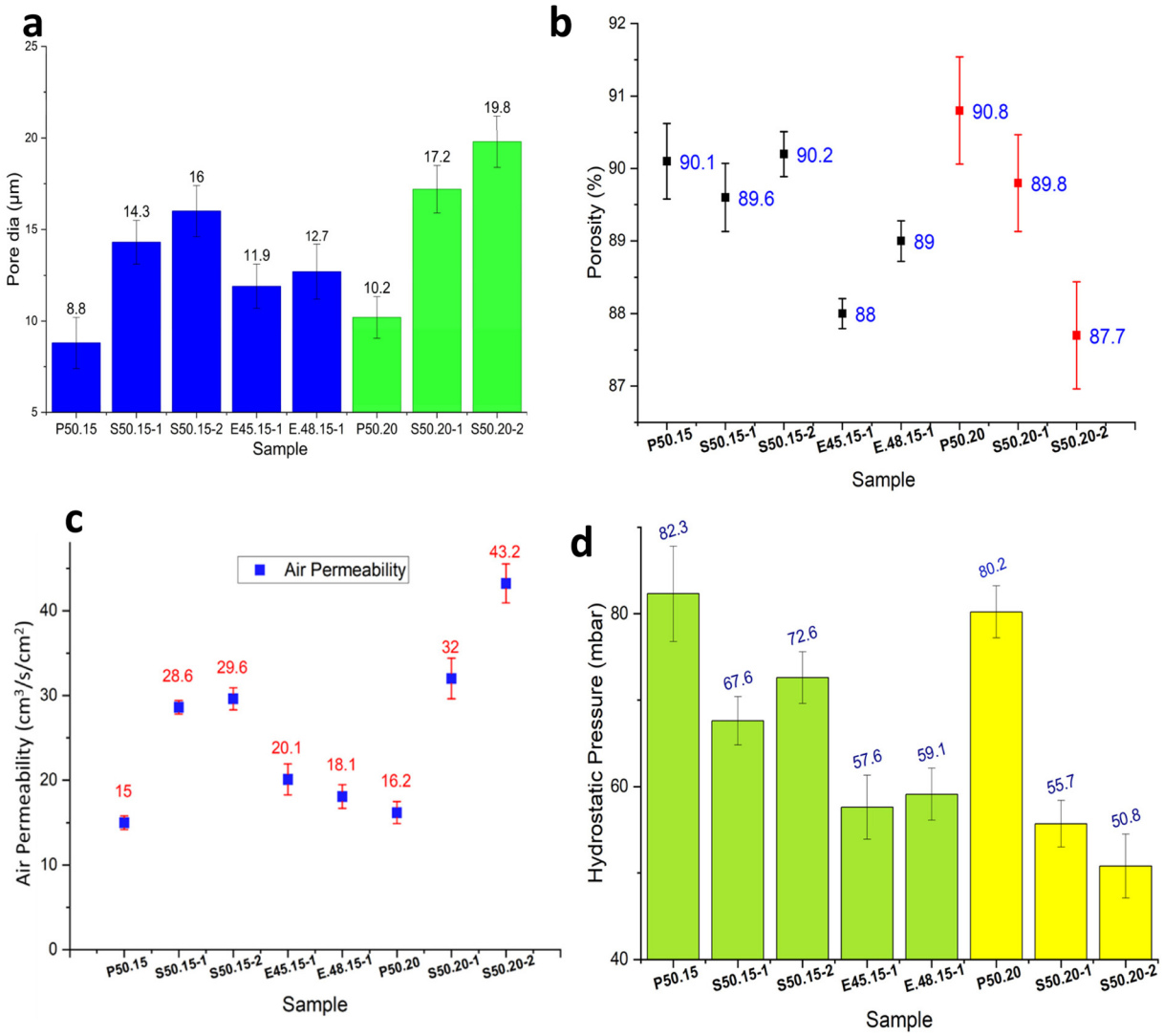

Fig. 7 (a) Mean pore diameter of produced melt-blown webs. (b) Porosity of produced melt-blown webs. (c) Mean air permeability of produced melt-blown nonwovens. (d) Mean hydrostatic pressure of produced melt-blown nonwovens.

incorporation of MgSt. As shown in Fig. 7c, sample S50.20-2 showed the highest air permeability of 43 cm^3 s^{-1} cm^{-2}, whereas the PP sample P50.15 displayed the lowest value at 15 cm^3 s^{-1} cm^{-2}. Overall, the addition of MgSt resulted in nearly a twofold increase in air permeability across comparable samples. This enhancement is closely related to changes in pore structure. The average pore diameter of S50.20-2 (19.2 μm) was more than double that of P50.15 (8.8 μm), while the fiber diameters of the two samples remained similar at 3.4 μm and 3.5 μm, respectively. Because fiber size alone cannot account for the large change in airflow, the increased pore size and more open web architecture in MgSt-containing samples are the primary contributors to the improved air permeability. The more loosely packed fiber network facilitates easier air passage through the web, aligning with the SEM observations and porometry data.

Collectively, these results demonstrate that MgSt alters the consolidation behavior of PP during melt-blowing, generating webs with larger interconnected pores and substantially higher air permeability without compromising fiber uniformity.

Hydrostatic pressure. In the case of samples with additives, it has been found that the hydrostatic head ranges from 51 to 82 mbar as presented in Fig. 7d. This range is significantly lower compared to samples without additives, indicating a reduced resistance to water penetration. By examining SEM images and from air permeability data, results show that the samples with additives possess a less compact structure. Consequently, this changed structure contributes to their decreased liquid barrier properties and results in lower hydrostatic head value. The resistance of nonwoven material to liquid increases as its average pore size decreases. When the

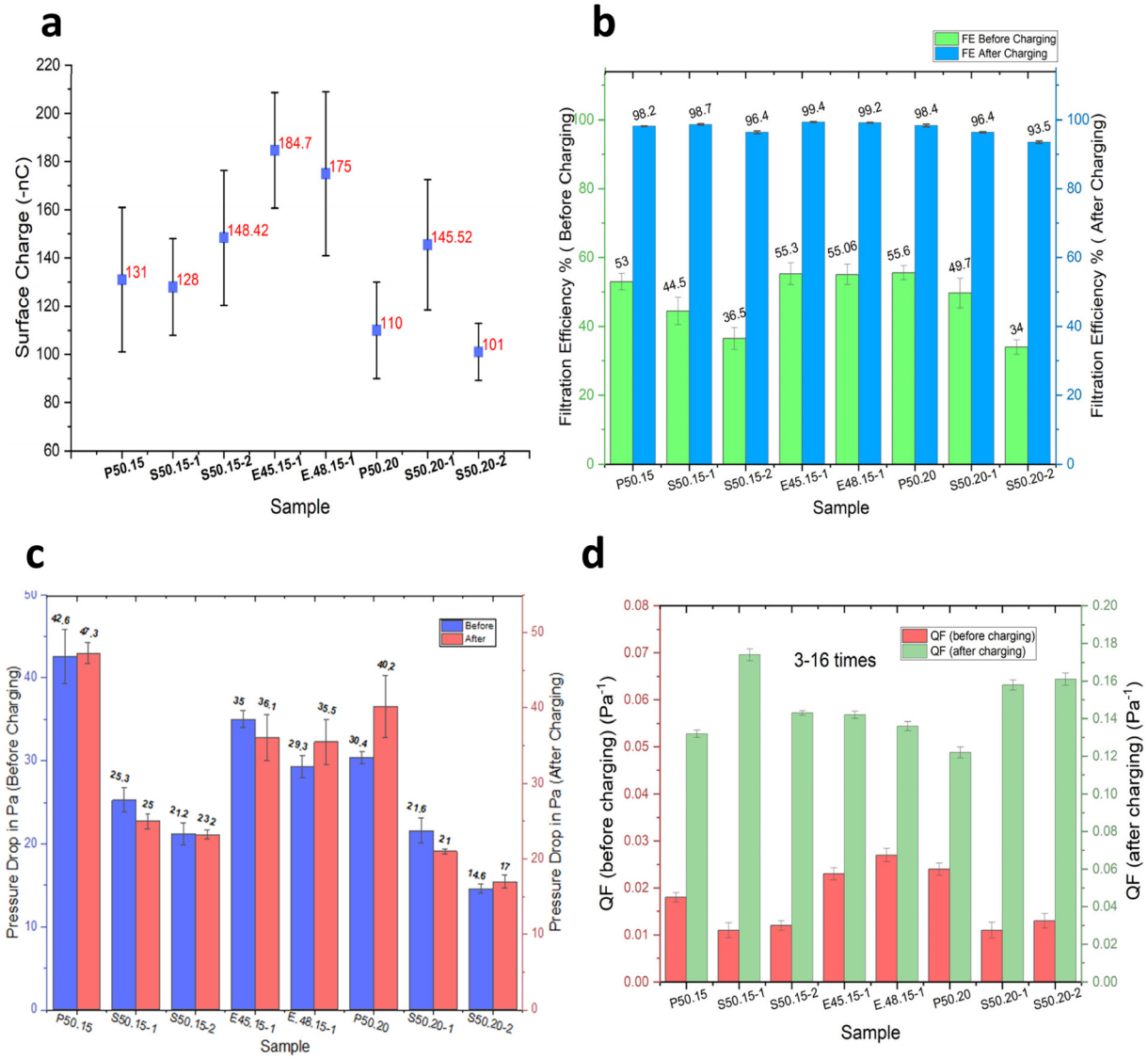

Fig. 8 (a) Surface charge of samples produced with and without MgSt. (b) Effect of corona charging on filtration efficiency of MB. (c) Pressure drops before and after the corona treatment of MB and (d) quality factor of melt-blown nonwovens.

pores are smaller, liquids encounter more difficulty penetrating or flowing through the fabric. As a result, there is an increase in the hydrostatic head.[34]

Surface charge. The corona charging was conducted under specific conditions, with a fixed voltage of −50 kV and a constant speed of 2 m min^{-1}. The distance between the corona discharge electrode and the sample surface was maintained at 7 cm throughout the experiment. The resulting average surface charge measured in this study ranged from −101 nC to −184 nC. Measurements revealed that samples containing additives exhibited a higher magnitude of charge compared to those without additives (Fig. 8a). This indicates that the inclusion of the additive has enhanced or facilitated the charge development during corona treatment.

Filtration efficiency and pressure drop. To improve particle filtration performance, corona charging technology was used to enhance the electrostatic capture mechanism. Consequently, it is reasonable to assume that corresponding improvements in filtration performance occurred. In Fig. 8b, the charged PP sample had an FE ranging from 93.5% to 99.4%. When subjected to corona treatment, the FE increased by approximately 2 times. Conversely, the PP/MgSt samples had even better FE compared to the PP sample. By incorporating about 1 wt% of MgSt, an FE of 99.4% was achieved with a PD of 36 Pa. This suggests that the use of MgSt can enhance filtration performance through increased particle collection due to the increase in electrostatic force. The overall PD ranged from 17 to 47.3 Pa (Fig. 8c). It is worth noting that the addition of MgSt resulted in larger fiber diameter and mean pore diameter, which translates into less breathing resistance. To evaluate the FE and PD of MB samples, their QF values were calculated. The results showed that adding MgSt particles to the samples improved their QF. This is because MgSt offers better FE and lower PD. Among all tested samples, S50.15.1 performed best with a QF value of 0.174, surpassing all other variations (Fig. 8d). The QF is significantly higher (p value is less than 0.05) than it is for uncharged samples.

Filtration and electret properties. The stability of the FE is a crucial property for electret filtration materials. Over time, the charges in the material tend to be attenuated, leading to a decline in FE. After forming electrets, the stability of the FE for both the samples with and without MgSt was investigated by measuring the FE as a function of storage time. The analysis involved taking measurements every 15 days to investigate any changes or variations in FE during the study. Fig. 9 illustrates that the FE of the pure PP samples (P50.15 and P50.20) decreased markedly by approximately 5.7% and 6%, respectively, after 60 days. In contrast, the PP samples containing 1 wt% and 2 wt% MgSt exhibited only a minor reduction of about 1–1.5%. These results indicate that the incorporation of MgSt significantly enhances the long-term stability of the FE in PP-based materials. Compared to materials with no additives, the charge retention improved by 42% after 60 days.

In fact, as the concentration of MgSt increased, the decline in FE decreased significantly. Increasing the MgSt concentration in PP does not inherently decrease FE but optimized doping with MgSt can enhance and stabilize it by improving the electret properties, which increase charge retention and particle capture. However, as shown in Fig. 9, beyond 1 wt%, further increments of MgSt do not provide additional benefits and sometimes causes a steady or even diminishing FE, indicating a saturation point for the positive effect of MgSt. When

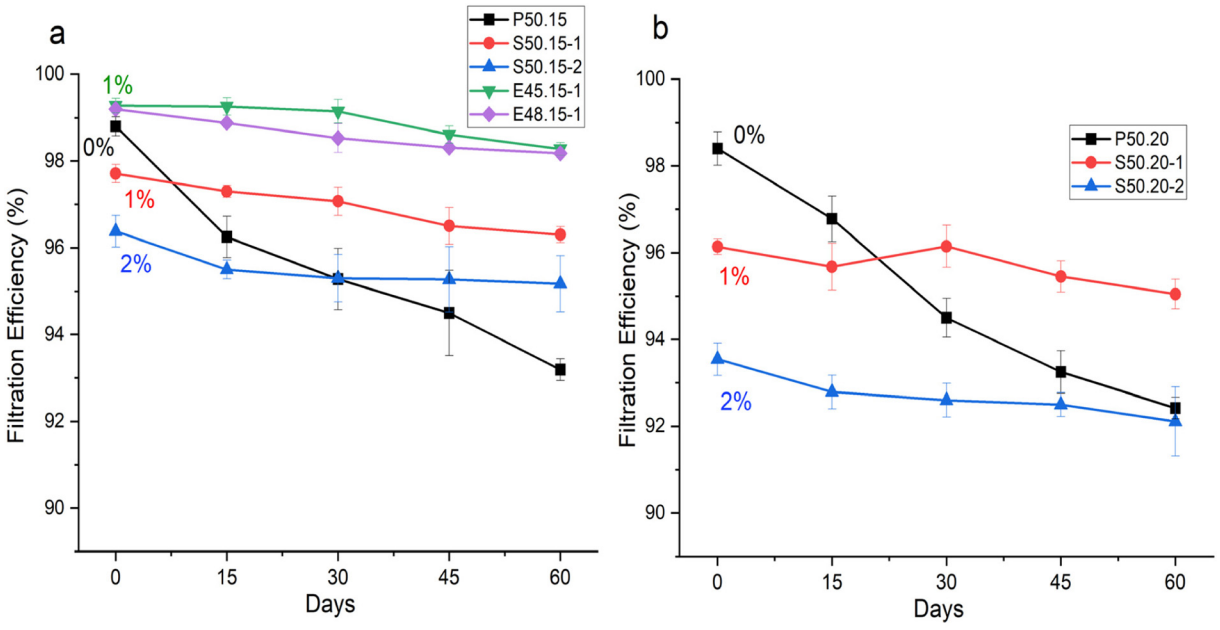

Fig. 9 Changes in Filtration Efficiency Over Time: (a) Samples With and Without Additives Produced at 15 cm DCD; (b) Samples With and Without Additives Produced at 20 cm DCD.

the amount of MgSt exceeds the optimal concentration, both FE and charge retention reach a plateau, where the structure cannot benefit significantly. Excess MgSt can interfere with the melt-blown fiber structure, potentially causing agglomeration or a defective morphology, which can slightly reduce FE.[35–37]

The mechanism of improving the electret properties. The electret stability of PP is influenced by its degree of crystallinity. Higher crystalline rates generally improve charge retention by reducing charge mobility and providing deeper, more stable trap sites at the interfaces between crystalline and amorphous regions. The dense, ordered crystalline domains act as physical and energetic barriers that reduce charge diffusion and suppress leakage. Conversely, the interfacial regions work as effective deep traps that need significant thermal energy for charge decay. As a result, PP melt-blown with higher crystallinity exhibits slower charge decay and greater thermal and humidity stability. The dominant mechanism governing this behavior is the restricted charge transport due to crystalline barriers and the presence of deep interfacial traps that stabilize the stored charges over time.[38]

To investigate the possible mechanisms of MgSt particles enhancing electret performance, the crystal structures and various crystal parameters were calculated using DSC and XRD experiments. This study demonstrates that the inclusion of MgSt in the samples enhanced charge stability by effectively capturing more charges within deeper traps. Consequently,

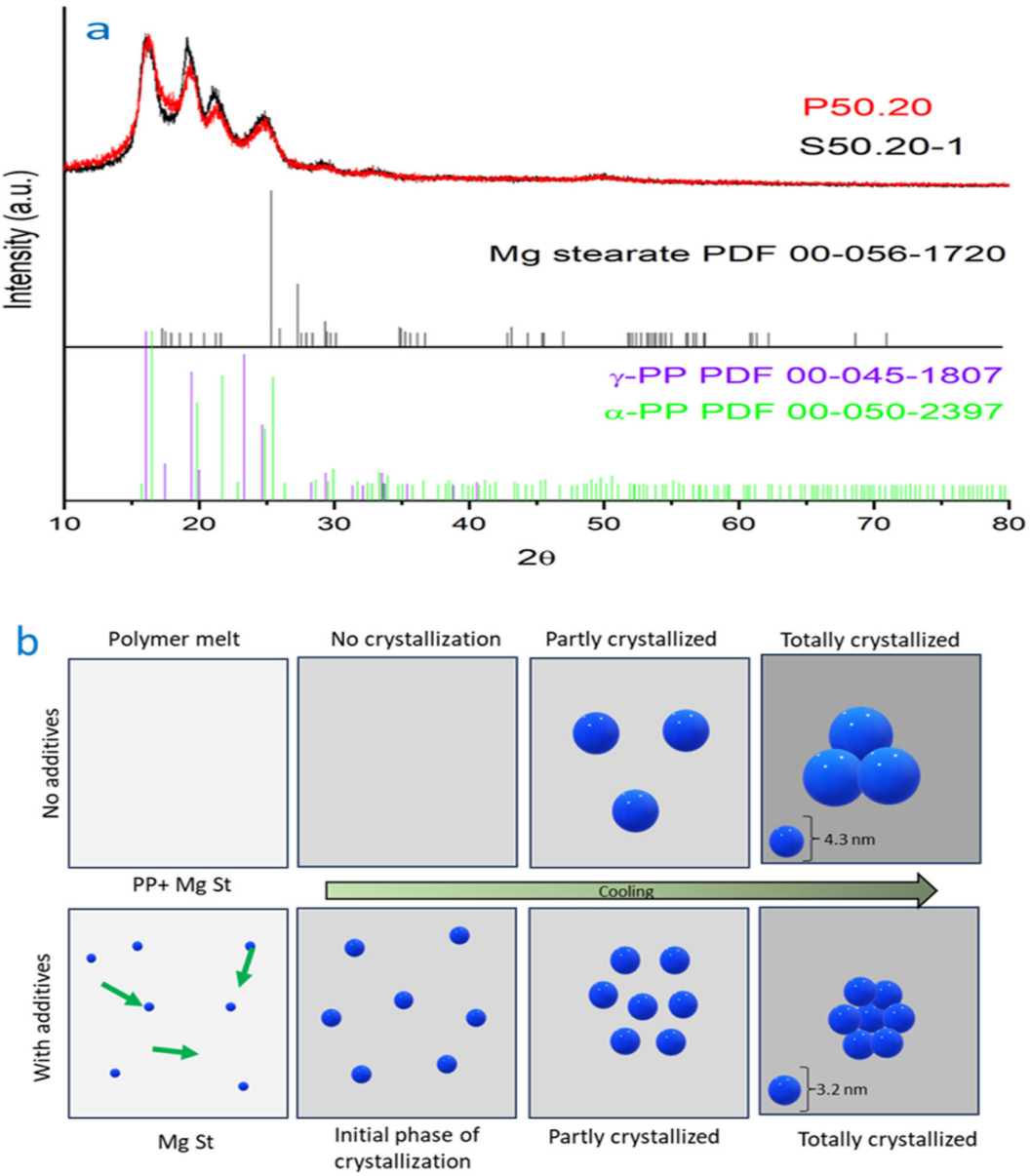

Fig. 10 The crystal structures of the PP/MgSt melt-blown nonwovens. (a) XRD diffraction pattern of PP/MgSt nonwovens. (b) The crystal formation process for the pure PP melt-blown nonwoven and the PP/MgSt samples.

these trapped charges were less likely to escape, contributing to the superior charge stability exhibited by the samples containing MgSt. The pure PP sample exhibits a crystallinity of 41%, as determined by DSC (Fig. S2). However, the addition of 1 wt% MgSt to the sample leads to an increase in crystallinity up to 42%. This observation suggests that incorporating MgSt enhances the formation of crystalline structures within the material. Additionally, it is found that although there is a slight delay compared to pure PP polymer, the presence of MgSt accelerates the overall crystallization process. Specifically, with MgSt present, the completion of crystallization occurs at a lower temperature of approximately 5 °C compared to that for pure PP. Moreover, the cooling stage demonstrates sharper peak(s), further supporting enhanced development and more rapid progress in crystallization due to the inclusion of magnesium stearate. Additionally, the X-ray diffraction (XRD) patterns are depicted in Fig. 10a, and additional crystal parameters have been provided in the SI. The XRD analysis revealed a difference between the intensity peak for the sample containing MgSt compared to pure PP. Specifically, the presence of MgSt resulted in sharper peaks with greater intensity. This finding suggests that MgSt plays a role in improving crystallinity within the sample. To further support their findings, the average crystallite (grain) size was calculated using the Scherrer equation. As seen in Fig. 10b, the sample with MgSt showed a smaller average crystal size of 3.2 nm, whereas the pure PP showed a slightly larger crystal size of 4.3 nm. The inclusion of MgSt as an additive has resulted in generating a more refined morphology. The results indicated that without the presence of MgSt, crystal nuclei formation relies on molecular motion, leading to a slow nucleation rate and the growth of large spherical sizes. However, heterogeneous nucleation occurs abundantly when nucleating agents like MgSt were introduced into the system. This promoted collisions between spherulites and hinders their growth due to insufficient time for expansion.[8] Whereas small crystallinity differences are observed with additives, which may make some contribution to charging stability, there may be other factors involved as well, and these need to be further investigated.

Conclusion

A straightforward yet efficient approach was introduced to create high-performance air filters by integrating the melt-blown technique with corona charging treatment. This study primarily examined the impact of charging distance on filtration performance, revealing that a distance of 7 cm yields the highest FE under the conditions investigated. Adding MgSt resulted in electret melt-blown with exceptional FE and minimal air resistance. This was accomplished through the strategic control of melt-blowing process parameters as well, resulting in a fluffy nonwoven filter featuring fine fiber diameter, small pore size, and high porosity. Also, increasing the additive concentration beyond 1% did result in reduced filtration performance due to the fact that the web structure changed because of change in fiber diameter. Processability is also affected by the addition of the charge enhancer, requiring further process optimization. The research findings demonstrated remarkable results in terms of filtration performance and achieving a high FE reaching up to 99.4%, low PD measuring only 17 Pa, and a higher QF value of 0.175 Pa^{-1} at an air flow rate of 32 L min^{-1}. Overall, the FE and quality of the produced melt-blowns are comparable to, or sometimes better than, those of commercially available melt-blowns. Considering the fact that it was possible to achieve a required FE with lower PD for many samples of 35 g m^{-2}, it may be possible to reduce the weight of the fabric and achieve the required performance, which may lead to savings in weight and cost of the material. Thus, it may be possible to change the structure of melt-blown filter media by appropriate process optimization depending on the needs for desired applications. Future work should further explore the humidity-dependent charge decay and long-term aging behavior of MgSt-modified melt-blown under both ambient and accelerated environmental conditions to better predict real-world performance. Extending the storage period beyond 60 days and testing against biologically relevant aerosols or real PM pollution would further validate durability and application readiness.

Author contributions

The manuscript was written through equal contributions of all authors. All authors have given approval to the final version of the manuscript.

Conflicts of interest

The authors declare no conflict of interest.

Data availability

The data supporting this article have been included as part of this manuscript.

Supplementary information (SI) is available. See DOI: https://doi.org/10.1039/d5lp00221d.

References

1 N. Mahowald, Aerosol indirect effect on biogeochemical cycles and climate, *Science*, 2011, **334**(6057), 794–796, DOI: 10.1126/science.1207374.
2 C. Liu, P. C. Hsu, H. W. Lee, M. Ye, G. Zheng, N. Liu, *et al.*, Transparent air filter for high-efficiency PM2.5 capture, *Nat. Commun.*, 2015, **6**(1), 1–9. Available from: https://www.nature.com/articles/ncomms7205.
3 S. Zhang, H. Liu, N. Tang, S. Zhou, J. Yu and B. Ding, Spider-Web-Inspired PM0.3 Filters Based on Self-Sustained

Electrostatic Nanostructured Networks, *Adv. Mater.*, 2020, **32**(29), 2002361, DOI: 10.1002/adma.202002361.

4 L. Liao, W. Xiao, M. Zhao, X. Yu, H. Wang, Q. Wang, *et al.*, Can N95 Respirators Be Reused after Disinfection? How Many Times?, *ACS Nano*, 2020, **14**(5), 6348–6356, DOI: 10.1021/acsnano.0c03597.

5 R. Thakur, D. Das and A. Das, Electret Air Filters, *Sep. Purif. Rev.*, 2013, **42**(2), 87–129, DOI: 10.1080/15422119.2012.681094.

6 H. Zhang, N. Liu, Q. Zeng, J. Liu, X. Zhang, M. Ge, *et al.*, Design of Polypropylene Electret Melt Blown Nonwovens with Superior Filtration Efficiency Stability through Thermally Stimulated Charging, *Polymers*, **12**(10), 2341, Available from: https://www.mdpi.com/journal/polymers.

7 S. Sankhyan, K. N. Heinselman, P. N. Ciesielski, T. Barnes, M. E. Himmel, H. Teed, *et al.*, Filtration Performance of Layering Masks and Face Coverings and the Reusability of Cotton Masks after Repeated Washing and Drying, *Aerosol Air Qual. Res.*, 2021, **21**(11), 210117. Available from: https://aaqr.org/articles/aaqr-21-05-oa-0117.

8 H. Zhang, J. Liu, X. Zhang, C. Huang and X. Jin, Design of electret polypropylene melt blown air filtration material containing nucleating agent for effective PM2. 5 capture, *RSC Adv.*, 2018, **8**(15), 7932–7941, Available from: https://pubs.rsc.org/en/content/articlehtml/2018/ra/c7ra10916d.

9 A. Jackiewicz and L. Werner, Separation of Nanoparticles from Air Using Melt-Blown Filtering Media, *Aerosol Air Qual. Res.*, 2015, **15**(6), 2422–2435, DOI: 10.4209/aaqr.2015.04.0236.

10 R. Thakur, D. Das and A. Das, Optimization study to improve filtration behaviour of electret filter media, *J. Text. Inst.*, 2016, **107**(11), 1456–1462, DOI: 10.1080/00405000.2015.1128207.

11 R. Thakur, D. Das and A. Das, Optimization of charge storage in corona-charged fibrous electrets, *J. Text. Inst.*, 2014, **105**(6), 676–684, DOI: 10.1080/00405000.2013.844417.

12 D. Das, R. Thakur and A. K. Pradhan, Optimization of corona discharge process using Box–Behnken design of experiments, *J. Electrost.*, 2012, **70**(6), 469–473.

13 Y. Gao, B. X. Du, F. Y. Yan, K. Hou, Z. Y. Liu and J. D. Chai, Effects of charging temperature and charging time on surface potential decay of PTFE film with back electrode ungrounded, *Proc. - Int. Symp. Electrets*, 2011, 105–106.

14 A. Kilic, E. Shim and B. Pourdeyhimi, Electrostatic Capture Efficiency Enhancement of Polypropylene Electret Filters with Barium Titanate, *Aerosol Sci. Technol.*, 2015, **49**(8), 666–673, DOI: 10.1080/02786826.2015.1061649.

15 A. Kilic, E. Shim, B. Pourdeyhimi and B. Y. Yeom, Aerosol filtration properties of nucleating agent containing electret filters, *Polym. Eng. Sci.*, 2014, **54**(7), 1533–1539, DOI: 10.1002/pen.23693.

16 J. H. Lin, C. W. Lou and Z. Z. Yang, Novel Process for Manufacturing Electret from Polypropylene Nonwoven Fabrics, *J. Text. Inst.*, 2004, **95**(1–6), 95–105, DOI: 10.1533/joti.2002.0004.

17 R. Thakur, D. Das and A. Das, Study of charge decay in corona-charged fibrous electrets, *Fibers Polym.*, 2014, **15**(7), 1436–1443, DOI: 10.1007/s12221-014-1436-9.

18 B. Yu, J. Han, H. Sun, F. Zhu, Q. Zhang and J. Kong, The Preparation and property of poly(lactic acid)/tourmaline blends and melt-blown nonwoven, *Polym. Compos.*, 2015, **36**(2), 264–271, DOI: 10.1002/pc.22939.

19 A. Brochocka, K. Majchrzycka and K. Makowski, Modified Melt-Blown Nonwovens for Respiratory Protective Devices Against Nanoparticles, *Fibres Text. East. Eur.*, 2013, **100**(4), 106–111.

20 J. Feng, Preparation and properties of poly(lactic acid) fiber melt blown non-woven disordered mats, *Mater. Lett.*, 2017, **189**, 180–183.

21 Y. Yesil and G. S. Bhat, Porosity and barrier properties of polyethylene meltblown nonwovens, *J. Text. Inst.*, 2017, **108**(6), 1035–1040, DOI: 10.1080/00405000.2016.1218109.

22 H. Xiao, J. Gui, G. Chen and C. Xiao, Study on correlation of filtration performance and charge behavior and crystalline structure for melt-blown polypropylene electret fabrics, *J. Appl. Polym. Sci.*, 2015, **132**(47), DOI: 10.1002/app.42807.

23 M. A. Hassan, B. Y. Yeom, A. Wilkie, B. Pourdeyhimi and S. A. Khan, Fabrication of nanofiber meltblown membranes and their filtration properties, *J. Membr. Sci.*, 2013, **427**, 336–344.

24 M. M. Uddin, B. Blevins, N. S. Yadavalli, M. T. Pham, T. D. Nguyen, S. Minko, *et al.*, Highly flexible and conductive stainless-steel thread based piezoelectric coaxial yarn nanogenerators via solution coating and touch-spun nanofibers coating methods, *Smart Mater. Struct.*, 2022, **31**(3), 035028, DOI: 10.1088/1361-665X/ac5015.

25 N. A. Shepelin, A. M. Glushenkov, V. C. Lussini, P. J. Fox, G. W. Dicinoski, J. G. Shapter, *et al.*, New developments in composites, copolymer technologies and processing techniques for flexible fluoropolymer piezoelectric generators for efficient energy harvesting, *Energy Environ. Sci.*, 2019, **12**(4), 1143–1176. Available from: https://pubs.rsc.org/en/content/articlehtml/2019/ee/c8ee03006e.

26 S. Chen, K. Li and S. Nijdam, Transition mechanism of negative DC corona modes in atmospheric air: from Trichel pulses to pulseless glow, *Plasma Sources Sci. Technol.*, 2019, **28**(5), 055017, DOI: 10.1088/1361-6595/aae554.

27 A. Bogaerts, E. Neyts, R. Gijbels and J. Van der Mullen, Gas discharge plasmas and their applications, *Spectrochim. Acta, Part B*, 2002, **57**(4), 609–658.

28 M. M. Bandi, Electrocharged facepiece respirator fabrics using common materials: Electrocharged fabrics, *Proc. R. Soc. A*, 2020, **476**(2243), 20469020, Available from: https://groups.oist.jp/nnp/electrocharge-mask.

29 X. Zhang, J. Liu, H. Zhang, J. Hou, Y. Wang, C. Deng, *et al.*, Multi-Layered, Corona Charged Melt Blown Nonwovens as High Performance PM0.3 Air Filters, *Polymers*, 2021, **13**(4), 485, Available from: https://www.mdpi.com/985674.

30 S. Bae, G. Ju, Y. Jang, *et al.*, Effect of Electret Process Parameters on Filtration Performance of Polypropylene

Melt-Blown Nonwoven Fabric, *J. Phys.:Conf. Ser.*, 2020, **1622**(1), 012049, DOI: 10.1088/1742-6596/1622/1/012049.

31 Z. Wang, Q. Song, H. Wu, B. Feng, Y. Li and L. Bu, Synchronized 3D Printing and Corona Charging for One-Step Prototyping of Polarized Polylactic Acid Electrets, *Polymers*, 2023, **15**(11), 2520.

32 B. Yu, J. Han, X. He, G. Xu and X. Ding, Effects of Tourmaline Particles on Structure and Properties of Polypropylene Filtration Melt-Blown Nonwoven Electrets, *J. Macromol. Sci., Part B*, 2012, **51**(4), 619–629.

33 X. Zhu, Z. Dai, K. Xu, Y. Zhao, Q. Ke, X. Zhu, *et al.*, Fabrication of Multifunctional Filters via Online Incorporating Nano–TiO2 into Spun–Bonded/Melt–Blown Nonwovens for Air Filtration and Toluene Degradation, *Macromol. Mater. Eng.*, 2019, **304**(12), 1900350, DOI: 10.1002/mame.201900350.

34 Y. Yesil and G. S. Bhat, Porosity and barrier properties of polyethylene meltblown nonwovens, *J. Text. Inst.*, 2017, **108**(6), 1035–1040, DOI: 10.1080/00405000.2016.1218109.

35 Y. Zhao, Y. Zhang, J. Ju, Z. Qian, X. Cui, S. Wang, *et al.*, Stearate and hindered amine light stabilizers coordinate to boost charge storage performance of water electret melt-blown nonwovens, *Sep. Purif. Technol.*, 2024, **332**, 125729. Available from: https://www.sciencedirect.com/science/article/abs/pii/S1383586623026370.

36 H. Zhang, N. Liu, Q. Zeng, J. Liu, X. Zhang, M. Ge, *et al.*, Design of Polypropylene Electret Melt Blown Nonwovens with Superior Filtration Efficiency Stability through Thermally Stimulated Charging, *Polymers*, **12**(10), 2341, Available from: https://www.mdpi.com/journal/polymers.

37 G. S. Larsen, Y. Cheng, L. L. Daemen, T. N. Lamichhane, D. K. Hensley, K. Hong, *et al.*, Polymer, Additives, and Processing Effects on N95 Filter Performance, *ACS Appl. Polym. Mater.*, 2021, **2021**, 1022–1031, DOI: 10.1021/acsapm.0c01294.

38 A. Thyssen, K. Almdal and E. V. Thomsen, Electret stability related to the crystallinity in polypropylene, *IEEE Trans. Dielectr. Electr. Insul.*, 2017, **24**(5), 3038–3046. Available from: https://ieeexplore.ieee.org/document/8120362.